

FINITE ELEMENT MECHANICS ANALYSIS OF GROWTH AND INVASION
OF PANCREATIC DUCTAL ADENOCARCINOMA (PDAC)

A Thesis

Submitted to the Faculty

of

Purdue University

by

Ann Katharine Steele

In Partial Fulfillment of the

Requirements for the Degree

of

Master of Science

May 2020

Purdue University

West Lafayette, Indiana

THE PURDUE UNIVERSITY GRADUATE SCHOOL
STATEMENT OF THESIS APPROVAL

Dr. Bumsoo Han, Chair

School of Mechanical Engineering

Dr. Thomas Siegmund

School of Mechanical Engineering

Dr. Tonglei Li

School of Industrial and Physical Pharmacy

Approved by:

Dr. Nicole Key

Head of the School Graduate Program

ACKNOWLEDGMENTS

This work would not have been possible without the continuous support and guidance of my advisor, Dr. Bumsoo Han. I am sincerely grateful for his immense knowledge, enthusiasm and patience throughout all stages of my research and writing.

I also want to thank my committee members for their insightful comments and encouragement.

I am grateful to my labmates in the Biotransport Phenomena Group for their expertise, friendship and constant willingness to help.

Lastly, I sincerely thank my family: my parents Chris and Debbie Steele, my sister Mary and my grandparents, especially my grandmother Katharine Steele and late grandfather Richard Steele, for their support throughout my life and for always encouraging me to pursue higher education.

TABLE OF CONTENTS

	Page
LIST OF FIGURES	v
ABBREVIATIONS	vii
ABSTRACT	viii
1. INTRODUCTION	1
2. COMPUTATIONAL METHODS	5
2.1 Computational geometry	5
2.2 Assigning biomechanical properties to the FE model	6
2.3 <i>In vivo</i> boundary conditions	9
3. RESULTS	10
3.1 Control case	10
3.2 Effect of basement membrane thickness	11
3.3 Effect of basement membrane stiffness	13
3.4 Effect of local weakening of basement membrane	14
3.5 Effect of duct radius	15
3.6 Summary of key findings	18
4. DISCUSSION	20
5. CONCLUSION	23
REFERENCES	24

LIST OF FIGURES

Figure	Page
1.1 Summary of the major cell types and growth and invasion dynamics involved in the development of epithelial cancers.	2
2.1 Mesh used for simulation, zoomed in incrementally. Left image shows overall mesh; middle image shows mesh on epithelial layer; right image shows mesh on basement membrane. Domains of model labeled in yellow, boundary conditions labeled in blue.	6
2.2 Load curve used to prescribe volumetric growth rate of tumor region. Dashed lines indicate time points where data was sampled.	8
3.1 Summary table of experimental cases and associated variations in properties.	10
3.2 Results of base "control" case. (a) - Development of 1st principal stresses [kPa] over time. (From left to right) initial time point, halfway time point, and end time point. (b) - Close-ups of stresses at end time point at intersection point of all domains. (c) - Total displacement [μm] at end time point.	11
3.3 Results of study into effect of basement membrane thickness. 1st principal stresses at end time point [kPa] - top 3 images show the radial stress profile at the bottom edge of model for (top to bottom) no BM, control case, and 500 nm BM. Bottom 3 images show the stress profile at the intersection point of all domains for (left to right) no BM, control case, and 500 nm BM.	12
3.4 Results of study into effect of basement membrane stiffness. 1st principal stresses at end time point [kPa] - top 3 images show the radial stress profile at the bottom edge of model for (top to bottom) 1 kPa, control case, and 100 kPa. Bottom 3 images show the stress profile at the intersection point of all domains for (left to right) 1 kPa, control case, and 100 kPa.	14
3.5 Results of study into effect of local weakening of basement membrane. Top image shows profiles for local degradation used in each case - (a) in blue and (b) in red. Bottom image shows the observed 1st principal stresses [kPa] at the end time point along the lower edge of model.	16

Figure	Page
3.6 Results of study into effect of duct radius. 1st principal stresses at end time point [kPa] - top 3 images show the radial stress profile at the bottom edge of model for (top to bottom) 1 mm lumen radius, control case, and 5 mm lumen radius. Bottom 3 images show the stress profile at the intersection point of all domains for (left to right) 1 mm lumen radius, control case, and 5 mm lumen radius.	17
3.7 Histograms comparing maximum 1st principal and shear stresses observed for each model case.	19

ABBREVIATIONS

PDAC	Pancreatic ductal adenocarcinoma
ECM	Extracellular matrix
CAF	Cancer-associated fibroblast
PSC	Pancreatic stellate cell
α -SMA	Alpha-smooth muscle actin
FGF	Fibroblast growth factor
IGF	Insulin-like growth factor
HGF	Hepatocyte growth factor
CXCL12	C-X-C motif chemokine 12
EMT	Epithelial-mesenchymal transition
TGF- β	Transforming growth factor beta
MMP	Matrix metalloproteinase
FEM	Finite element method
FEBio	Finite elements for biomechanics

ABSTRACT

Steele, Ann K. M.S., Purdue University, May 2020. Finite Element Mechanics Analysis of Growth and Invasion of Pancreatic Ductal Adenocarcinoma (PDAC). Major Professor: Bumsoo Han.

Here we describe a finite element model of the mechanical stresses and strains involved in the growth and development of epithelial cancers, specifically pancreatic ductal adenocarcinoma (PDAC). We model a growing tumor swelling over time, modeled as fluid influx in response to changing solute concentrations. Stresses and strains are computed in surrounding material regions in response to this swelling. Further studies are conducted into the relative impacts of factors such as basement membrane thickness, stiffness, and duct radius. We observe that normal stresses are confined mostly to the basement membrane layer and hypothesize that there exists some threshold for axial stress beyond which the basement membrane ruptures and cancer is able to invade into the surrounding tissue.

1. INTRODUCTION

Pancreatic ductal adenocarcinoma (PDAC) is the most common form of pancreatic cancer, accounting for more than 90% of cases worldwide [1]. It is also characterized by a strikingly poor prognosis with an overall 5-year survival rate of less than 8%. Despite the fact that PDAC is responsible for the fourth most cancer deaths annually [2], there are still gaps in our understanding of its mechanisms. This is especially true with respect to the mechanical forces involved in the cancer's growth and invasion. In this study, we aim to quantify the relative impact of various parameters affecting the mechanical force balance on a growing cancer tumor and the stroma, especially as they relate to invasion of the cancer. We hope that an understanding of the roles various components play from a mechanical perspective could inform potential treatment approaches.

Figure 1.1 introduces the biology of the pancreatic duct and how it changes in the presence of malignancy. The hollow duct is lined with a single layer of cuboidal epithelial cells, below which lies a thin fibrous membrane which is called the basement membrane. Beyond the basement membrane is the stroma region, which includes of extracellular matrix (ECM) fibers and fibroblasts. After one or more epithelial cells spontaneously transitions into a tumor cell, growth of the tumor begins. As shown in the right image of Figure 1.1, the presence of cancer induces changes in the surrounding microenvironment: fibroblasts differentiate into cancer-associated fibroblasts (CAFs), and the ECM becomes stiffer and denser. If the tumor continues growing, it will eventually break through the basement membrane and invade the surrounding tissue, where cells may ultimately work their way into the bloodstream and spread to other parts of the body.

There is substantial knowledge related to the molecular mechanisms through which PDAC cells interact with their surrounding microenvironment. While PDAC cells

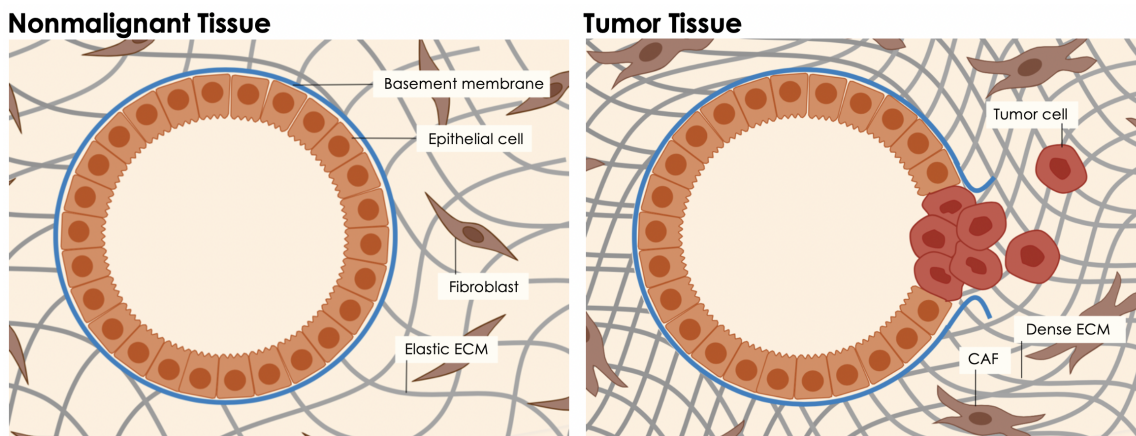


Figure 1.1. Summary of the major cell types and growth and invasion dynamics involved in the development of epithelial cancers.

are able to produce some ECM components on their own, they typically stimulate pancreatic stellate cells (PSCs) to produce them instead. Cytokines secreted by tumor cells activate the PSCs; activated PSCs are marked by α -smooth muscle actin (α -SMA) expression and work to produce the dense cancer-associated stroma [3]. A study by Olive et al. [4] found that in a mouse model of highly lethal, chemoresistant PDAC, stroma formation could be reduced by a hedgehog inhibitor. This reduction resulted in increased vascularization, increased delivery of therapeutic drugs and improved overall survival. Further studies of hedgehog inhibitors in murine models indicate that such inhibitors may be able to decrease desmoplastic stroma, increase vascularization and drug delivery to the tumor and decrease metastasis [5]. In humans as well the degree of α -SMA expression has been linked to prognosis [6]. Additional pathways involved in PDAC progression and invasion include fibroblast growth factor (FGF), insulin-like growth factor (IGF), hepatocyte growth factor (HGF) and others [3].

There have been a few studies attempting to better understand the mechanical and biophysical mechanisms associated with tumor-microenvironment interactions. As tumors grow, they strain the surrounding microenvironment and store strain energy [7]. Additionally, the stiffness of the surrounding stroma places some compressive

stresses on the tumor. A study from Jain et al. [8] involving growing cancer spheroids in agarose gels of varying concentrations found that compressive stresses inhibit tumor growth by increasing apoptosis through the mitochondrial pathway. They found that these effects are reversible and that nonuniformly applied compressive stresses can nonuniformly affect tumor cell proliferation and lead cells to proliferate primarily in the direction of least stress [8]. Work has been done which suggests that compressive stress increases the invasive phenotype of cancer cells as well as the expression of genes involved in ECM remodelling [9] [10]. Finally, although the biological purpose remains unknown, tumors are known to compress their own blood vessels as a result of generated solid stresses [11].

While the interactions and crosstalk between a growing tumor and its microenvironment are well documented from a chemical perspective [12] [13], we hope that further investigation of this relationship from a mechanical force balance perspective could provide valuable insight. The present study will focus on the time period when the tumor exists and is growing, but has not yet ruptured the basement membrane and spread beyond the epithelial layer. During this time, the stroma and its components are believed to play a combination role in the tumor's development - both promoting and suppressing its growth through different mechanisms. For example, CAFs produce various growth factors, chemokines, and cytokines which can foster angiogenesis, drug resistance and invasion [14], thereby promoting tumor growth, while the stiffened ECM and components may suppress tumor growth due to mechanical compression.

A 2016 review exploring the combination role of CAFs alone describes both their pro- and anti-tumorigenic functions in detail [15]. In addition to the angiogenic function listed above, high expression of chemokine ligand 12 (CXCL12) can induce epithelial-mesenchymal transition (EMT), migration and metastasis and tumor growth as well as impede the function of two immunological molecules which promote the function of T cells [16]. CAFs also secrete transforming growth factor- β (TGF- β), which induces EMT and can contribute to tumor growth and metastasis (reviewed

in [15]). The last key pathway through which CAFs promote tumor growth is via the degradation and remodeling of the ECM due to expression of MMPs. This remodeling facilitates tumor invasion, and physical remodeling allows cancer cells to follow in tracks created by Rho-ROCK activation by CAFs [17]. However, CAFs also exhibit some tumor-inhibiting effects. Secretion of TGF- β suppresses tumor initiation, and Flaberg et al. have shown that CAFs inhibit proliferation of cancer cells during *in vitro* co-culture [18].

This combination pro- and anti-tumorigenic role of the basement membrane and stroma is one of the most significant limitations of *in vivo*-based studies. Since they can only observe the overall phenomena resulting from the system as a whole, they are unable to separate the roles of specific components and properties of the microenvironment. This limitation can be addressed through the implementation of a computational model. With such a model, we are able to isolate or remove specific components and systematically vary model properties to understand the individual roles of selected components.

Here, we develop a biomechanics model of PDAC development and progression specifically focused on the mechanical stresses generated by tumor growth on the basement membrane and stroma tissue. In this pursuit, we will consider various forces involved in the growth process. Major factors include the outward growth of the tumor and resulting compression of the stroma, the preferential division of tumor and epithelial cells along the circumferential direction, the local degradation of the basement membrane due to secretions of matrix metalloproteinases (MMPs) and other enzymes. We will discuss each of these further as they are introduced to the model. One of the most significant innovations of this model is the use of a rate-controlled swelling of the tumor region to drive the deformation of surrounding tissue.

2. COMPUTATIONAL METHODS

In this study, we used the finite element method (FEM) to predict the stresses and deformations experienced by a growing tumor and its surrounding microenvironment. Recently, nonlinear elastic models can be implemented in FEM, allowing for analysis of soft tissue deformations. Here, a combination of materials models is used to analyze the forces and deformations involved in the growth of an epithelial tumor.

All models were implemented in Finite Elements for Biomechanics (FEBio), a free and publicly available software designed at the University of Utah for finite element analysis of biomechanical systems [19].

2.1 Computational geometry

The basic geometry of the pancreatic duct, including the epithelium, basement membrane and stroma was introduced in the previous section. To replicate these in an FE model, each layer was simplified to a concentric cylinder of constant inner and outer diameters. For the base model (control), the dimensions were assigned as follows: radius of ductal lumen $2000\ \mu\text{m}$ [20], thickness of epithelium $36\ \mu\text{m}$ [21], thickness of basement membrane $0.2\ \mu\text{m}$ [22]. The outer radius of the full geometry (including stroma) was chosen to be $2500\ \mu\text{m}$, which was assumed to be sufficiently large so that no deformation occurred on its outer edge.

A 45-degree wedge of the full 360-degree domain was chosen to simplify the required computations. A rectangular mesh, uniform across each layer, was implemented, yielding a total of 86,400 elements. The final geometry with mesh is shown in Figure 2.1.

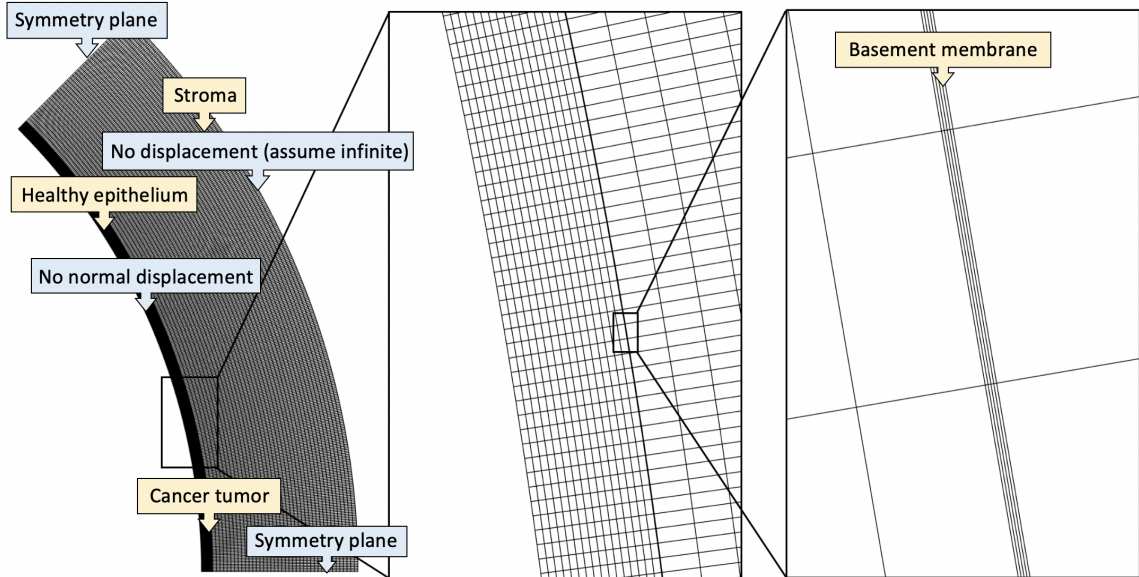


Figure 2.1. Mesh used for simulation, zoomed in incrementally. Left image shows overall mesh; middle image shows mesh on epithelial layer; right image shows mesh on basement membrane. Domains of model labeled in yellow, boundary conditions labeled in blue.

2.2 Assigning biomechanical properties to the FE model

Cancer cells were modeled as a homogeneous solid mixture of three materials – a soft linear elastic matrix to maintain the shape of all elements, an orthotropic elastic matrix to enforce the circumferential growth preference observed *in vivo*, and a concentration gradient-driven “cell growth” material. Material axes were defined elementwise to allow for material properties such as the orthotropic growth preference to be implemented in cylindrical coordinates.

Epithelial cells divide circumferentially around the duct rather than radially into or away from the lumen due to their polarity. Consequently, they experience much more circumferential strain and minimal radial strain as a group. This is the justification behind the use of an anisotropic stiffness matrix; by imposing a matrix which is softer along the circumferential axis than along the others we can facilitate elongation

primarily in this direction. A parametric study to investigate the sensitivity of the results to the assigned anisotropy ratio is attached in the supplementary materials.

The aforementioned cell growth material is responsible for driving all the deformation and stresses observed in the model. It represents a mechanism of volumetric growth, driven by the exchange of mass between the porous cell region and the surrounding environment. This mass can be any combination of solutes and water, all assumed to be incompressible. We assume that the interstitial fluid behaves ideally and that the solid matrix of the porous material exhibits negligible resistance to swelling. The main parameters required to define the model are:

c_r : the number of moles of membrane-impermeant solutes per initial reference volume

ϕ_r : the volume of the intracellular solid matrix with respect to the reference configuration

c_e : the osmolarity of the extracellular environment

Expansion of the cancer region is then governed by the relation:

$$p = R\theta\left(\frac{c_r}{J - \phi_r} - c^*\right) \quad (2.1)$$

Where p is the fluid pressure, J is the volume ratio of the porous solid matrix, R is the universal gas constant, θ is the absolute temperature and c^* is the osmolarity of the external environment.

The reference configuration refers to the stress-free initial configuration of the model, at the instant when the first epithelial cell has become malignant but has not yet begun to divide. To replicate the exponential cellular division and tumor growth with a prescribed doubling time, we can define load curves for c_r and ϕ_r such that they double in the desired amount of time. This is true since both quantities are normalized against the fixed reference configuration [23].

To mathematically ensure that the reference configuration is stress-free, we employ the following constraint:

$$c_r = (1 - \phi_r)c^* \quad (2.2)$$

Here, a doubling time of 159 days was chosen for both c_r and ϕ_r [24]. Further, we assume the extracellular osmolarity is constant at $c_e = 300$ mM, $\phi_r = 0.3$ initially, reflecting an intracellular matrix which occupies 30% of the cell volume. Each of these quantities is then set to double over the equivalent of 159 days. This is reflected in Figure 2.2, which shows the prescribed tumor growth curve, along with dashed red lines indicating the time points where data was sampled.

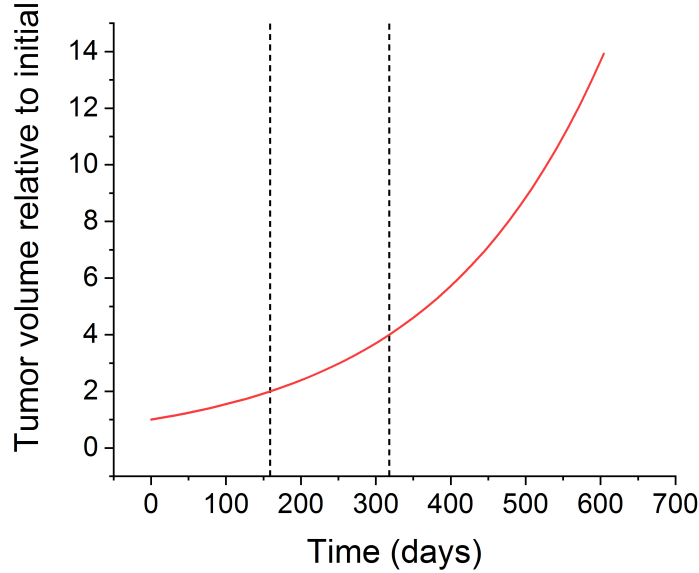


Figure 2.2. Load curve used to prescribe volumetric growth rate of tumor region. Dashed lines indicate time points where data was sampled.

All other material regions of the model are governed by a compressible Neo-Hookean constitutive model, whose strain energy density is given by

$$\Psi = \frac{G}{2}(I_1 - 3) - G \ln J + \frac{\lambda}{2}(\ln J)^2 \quad (2.3)$$

where the constants G and λ are material coefficients, $J = \det \mathbf{F}$ is the Jacobian of the deformation, and $I_1 = \text{tr} \mathbf{C}$, where \mathbf{C} is the right Cauchy-Green tensor. For each example, the material properties given will be Young's modulus E and Poisson's ratio ν , where $E = 2G(1 + \nu)$ and $\lambda = 2G\nu/(1 - 2\nu)$. We assumed equal densities and Poisson's ratios of 0.3 across these remaining domains. Elastic moduli of these regions were 0.87 kPa for the epithelium [25], 4 kPa for the stroma [26] and 10 kPa for the basement membrane [27].

2.3 *In vivo* boundary conditions

To fully constrain the model, boundary conditions were implemented as follows: symmetry planes were placed on the two slice (radial) planes. A no displacement condition was placed on the outermost edge of the stroma since we assume that surface to be sufficiently far from the deformed region to be considered quasi-infinite.

Lastly, a condition was placed on the inner surface of the lumen to enforce zero displacement normal to the selected surface; this allows for sliding along that plane but no penetration of it. In terms of the 2D velocity vector in polar coordinates $\mathbf{u} = (u, v)$, this can be expressed as

$$u = 0; \frac{\delta v}{\delta r} = 0 \tag{2.4}$$

for $r = r_0$, where r_0 is the inner radius of the lumen.

3. RESULTS

The general experimental design is summarized in Figure 3.1.

	BM thickness [nm]	BM stiffness [kPa]	Lumen radius [mm]
Case 0	200	10	2
Case 1	0	10	2
Case 2	500	10	2
Case 3	200	1	2
Case 4	200	100	2
Case 5	200	10	1
Case 6	200	10	5

Varied BM thickness

Varied BM stiffness

Varied lumen radius

Figure 3.1. Summary table of experimental cases and associated variations in properties.

3.1 Control case

First a control case was run to establish a baseline to which future data could be compared. The results of this model are shown in Figure 3.2. From these results, we can see that the growing cancer tumor compresses the epithelial layer circumferentially around the duct, with most of the normal stress contained within the basement membrane layer. The cancer region undergoes compression from the surrounding tissue, while the neighboring stroma and basement membrane undergo tension. Stress is propagated into the surrounding portion of the stroma as well.

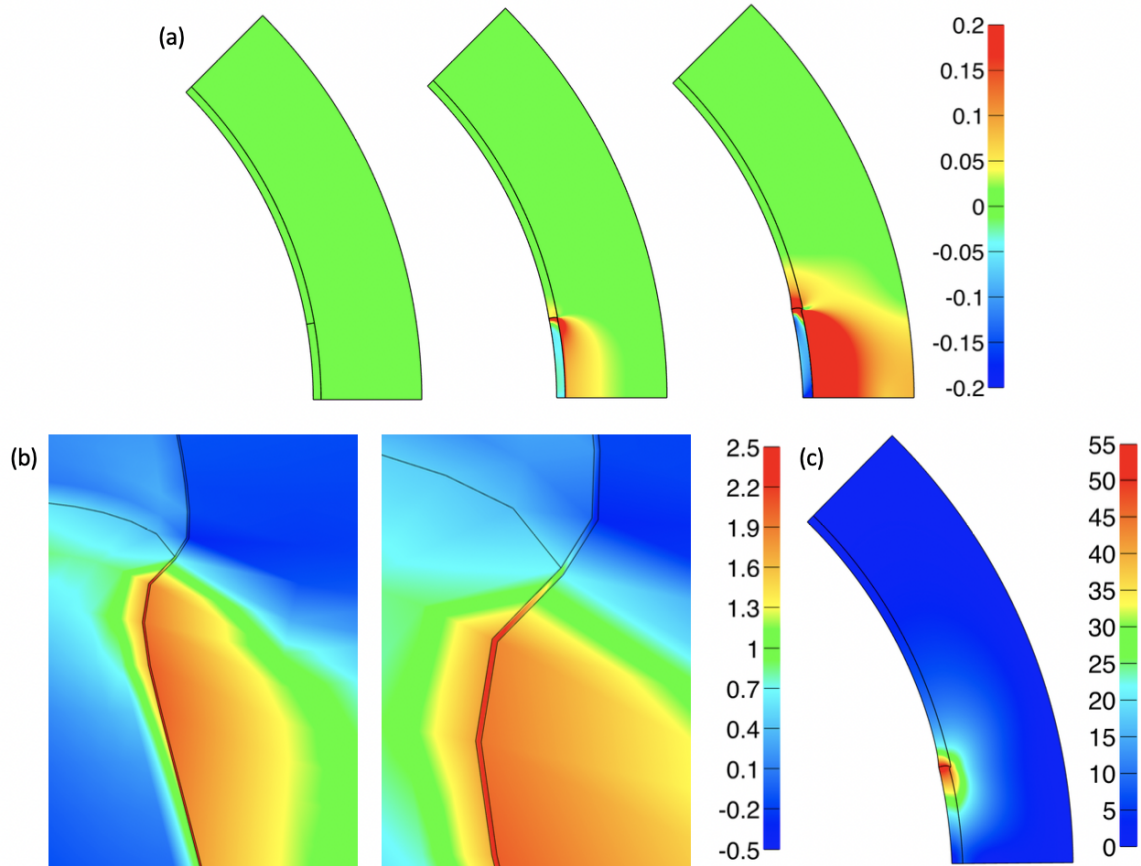


Figure 3.2. Results of base "control" case. (a) - Development of 1st principal stresses [kPa] over time. (From left to right) initial time point, halfway time point, and end time point. (b) - Close-ups of stresses at end time point at intersection point of all domains. (c) - Total displacement [μm] at end time point.

3.2 Effect of basement membrane thickness

The first comparison study that was run examined the effect of basement membrane thickness. Since the majority of normal stresses are confined to this layer, it made sense to examine the effect that its thickness had on the observed stress profile. The results of this study are shown in Figure 3.3. The first difference observed is that when the basement membrane is included (as in two of the three cases com-

pared here), it both absorbs a majority of stress and creates a layer of high stress in the neighboring domains. This is shown in the top half of Figure 3.3. This layer is not present when the basement membrane is omitted. However, the layer does not change significantly when thickness of the basement membrane is varied. The second difference observed between cases here is that the point in the stroma immediately bordering the intersection of cancer and healthy epithelial tissue undergoes an increasing degree of compression with increasing basement membrane thickness. This is shown in the bottom half of Figure 3.3. This pattern of stress indicates that the epithelial layer is exerting outward force on the stroma.

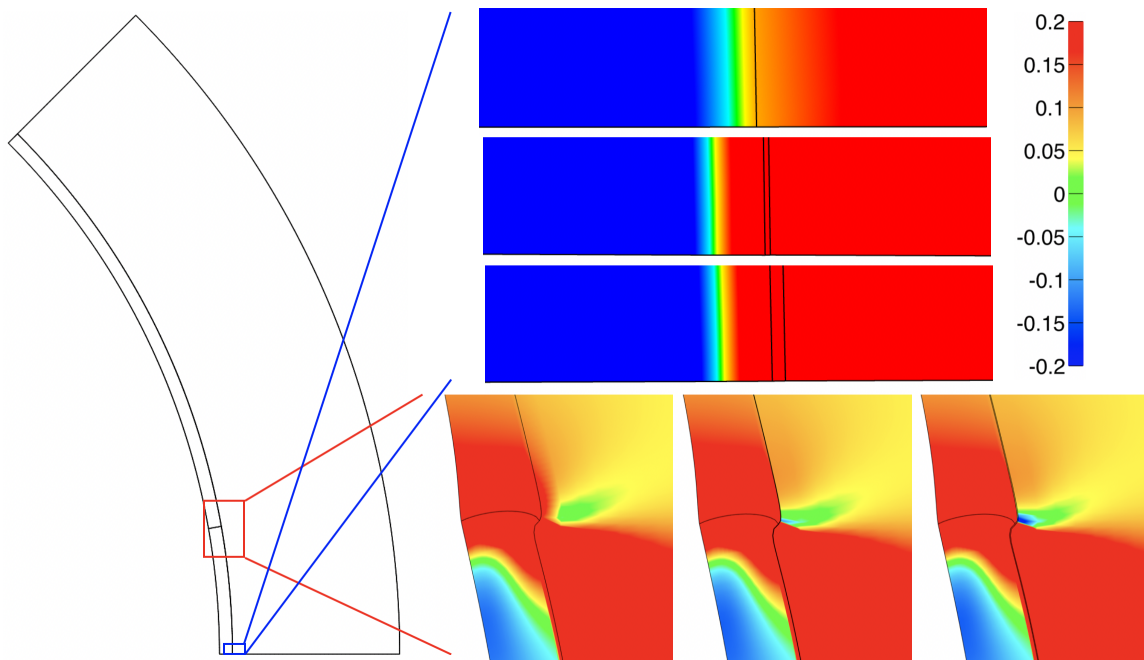


Figure 3.3. Results of study into effect of basement membrane thickness. 1st principal stresses at end time point [kPa] - top 3 images show the radial stress profile at the bottom edge of model for (top to bottom) no BM, control case, and 500 nm BM. Bottom 3 images show the stress profile at the intersection point of all domains for (left to right) no BM, control case, and 500 nm BM.

From a mechanics perspective, the observed phenomenon of stress concentration along the boundary between the cancerous epithelium and the basement membrane can be compared to uniform thermal loading of a bimetallic strip. In such cases, the strip is heated to some temperature other than the temperature the metals were bonded at and they begin to thermally expand at varying rates. This exerts normal and shear stresses on both members of the composite. Similarly, the expansion of the cancer tumor region we examine here exerts normal and shear stresses both on the tumor itself and on the basement membrane to which it is bonded. In the bimetallic strip case, it has been well documented that a concentration of principal stresses occurs at the boundary edge [28]. This appears to validate the presence of an edge effect layer of stress in our model.

3.3 Effect of basement membrane stiffness

The next study was to examine the effect of basement membrane stiffness. The justification for this inquiry is the same as the previous study. Results of this study are presented in Figure 3.4. Most significantly, as shown in the bottom half of the figure, a small spot in the stroma outside the intersection of cancer and epithelial regions experiences zero stress in the soft basement membrane case, then grows larger in the control case and finally undergoes some compression in the stiffer basement membrane case. This may indicate, as in the study of basement membrane thickness, that the stiffer basement membrane encourages the epithelial layer to press outward into the surrounding stroma. Additionally, in the top half of Figure 3.4 we can observe that the stiffening of the basement membrane leads to both a widening of the resulting boundary layer of stresses in the cancer region and a compaction of the gradient between this boundary layer and the zone outside of it. This stiff case represents a severe change in stress patterning compared to the resting state. We suspect that this change may promote anti-cancer response from the host tissue due to some signaling from the cancer cells undergoing this novel stress pattern.

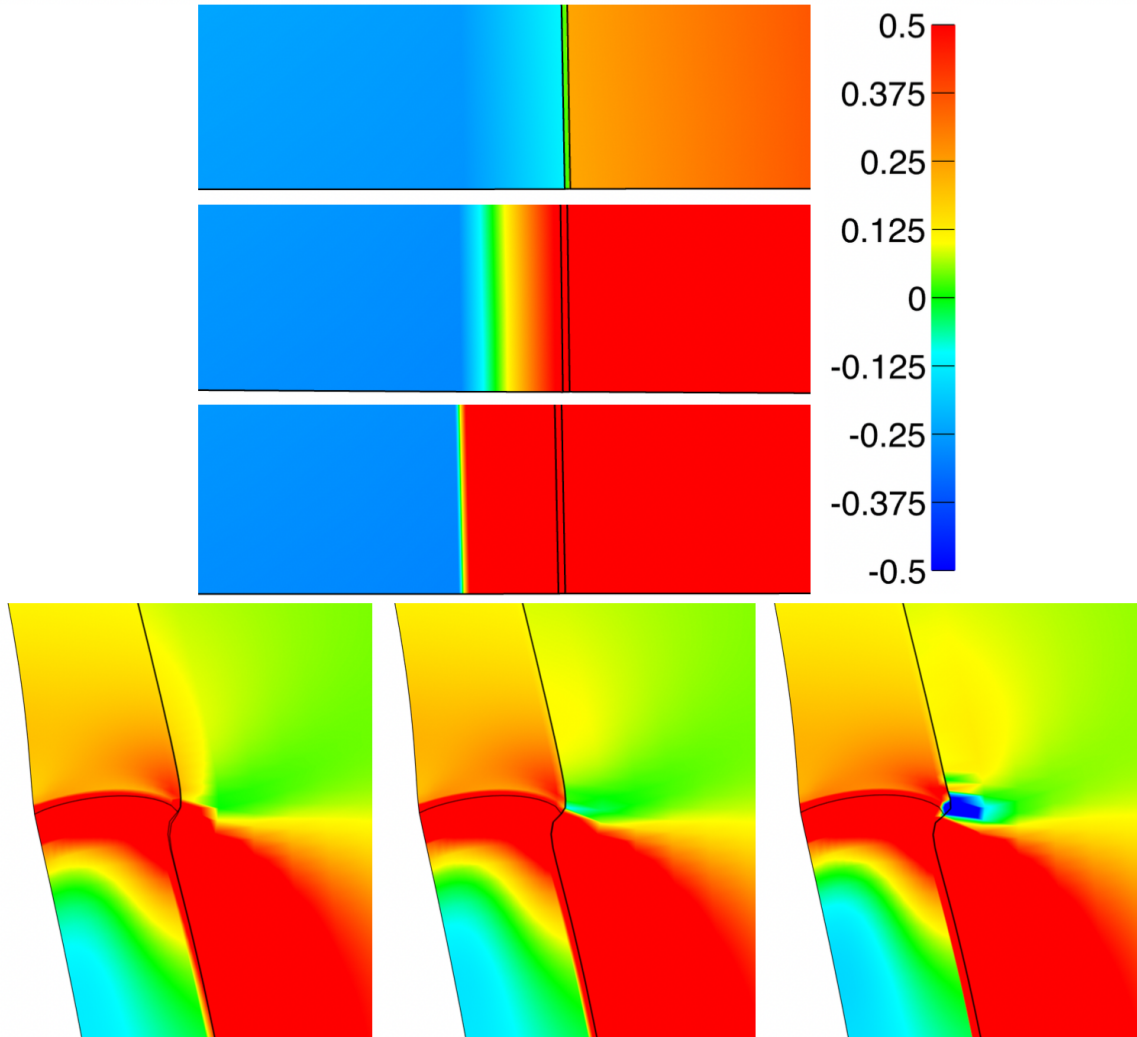


Figure 3.4. Results of study into effect of basement membrane stiffness. 1st principal stresses at end time point [kPa] - top 3 images show the radial stress profile at the bottom edge of model for (top to bottom) 1 kPa, control case, and 100 kPa. Bottom 3 images show the stress profile at the intersection point of all domains for (left to right) 1 kPa, control case, and 100 kPa.

3.4 Effect of local weakening of basement membrane

Next, we introduced a local weakening of the segment of the basement membrane which is in contact with the cancer region. It is known that degradation of the

basement membrane due to enzyme secretions plays a significant role in facilitating the invasion of cancer cells. This study explores two profiles for the degradation over time, which are presented alongside their accompanying results in Figure 3.5. The results of these two cases displayed no significant differences in the intersection region we have analyzed previously. However, as shown in the bottom half of Figure 3.5, at the model's bottom edge the differences between the cases are similar to those observed in Figure 3.4. That is, it seems that as the basement membrane begins to weaken, it results in lessening of stress beginning at the lower edge and presumably propagating upward.

3.5 Effect of duct radius

The final parameter we examined was the inner radius of the duct and its effect on the resulting stress profile. Some research has suggested that tumors originating in ducts of smaller radii are more prone to outward (exophytic) growth, while those originating in ducts of larger radii are more prone to inward (endophytic) growth [29]. To examine this, a set of models were constructed with large and small lumen radii. The results of this study are presented in Figure 3.6. In the top half of the figure, we can observe that at the bottom edge of the model, the stresses are less in the larger radius case. However, this is likely due to the fact that the bottom edge is located farther from the intersection point where the deformation is centered. Otherwise, the cases appear similar in terms of boundary layer thickness, stress gradient and others. In the bottom half of Figure 3.5, we can see the stress patterning at the intersection point. In the smaller duct case, there is less stress on the healthy epithelium and there is compression at the point in the stroma closest to the intersection. As the lumen radius increases, stress on the healthy epithelium increases and stress on the stroma in this region transitions through zero toward a small degree of tension. These findings appear to support the research mentioned above, that cancers in smaller ducts are more likely to experience outward growth into the stroma.

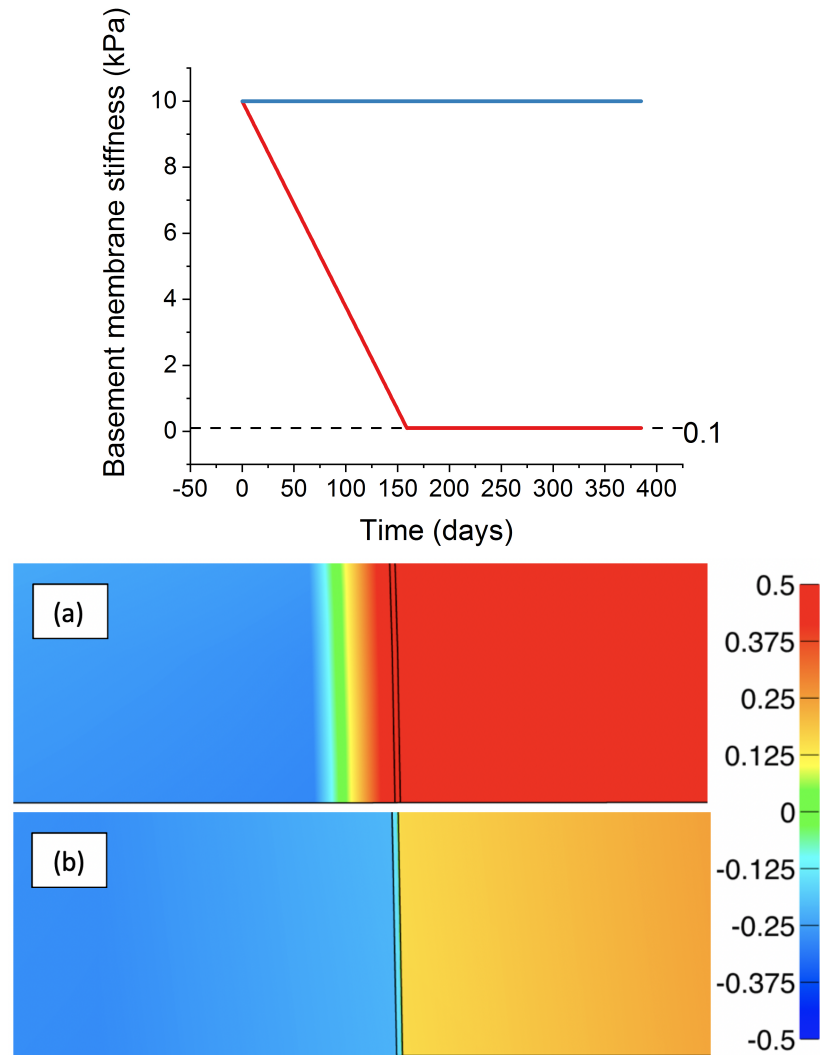


Figure 3.5. Results of study into effect of local weakening of basement membrane. Top image shows profiles for local degradation used in each case - (a) in blue and (b) in red. Bottom image shows the observed 1st principal stresses [kPa] at the end time point along the lower edge of model.

From a mechanics perspective, the phenomena of endo- and exophytic growth can be examined as a stability issue. Under this assumption, endophytic growth could be described as a global buckling inward and exophytic growth as a global buckling outward. As the cancer tumor grows and elongates, it undergoes a compressive load which could ultimately cause it to buckle. This problem is further complicated by

the curvature of the region and the presence of the stiff basement membrane layer to which the compressed cancer region is bonded. In this way, the problem can be thought of as a curved beam on a stiffer elastic Winkler-type foundation. This problem has been considered in literature and a detailed analysis is presented in [30].

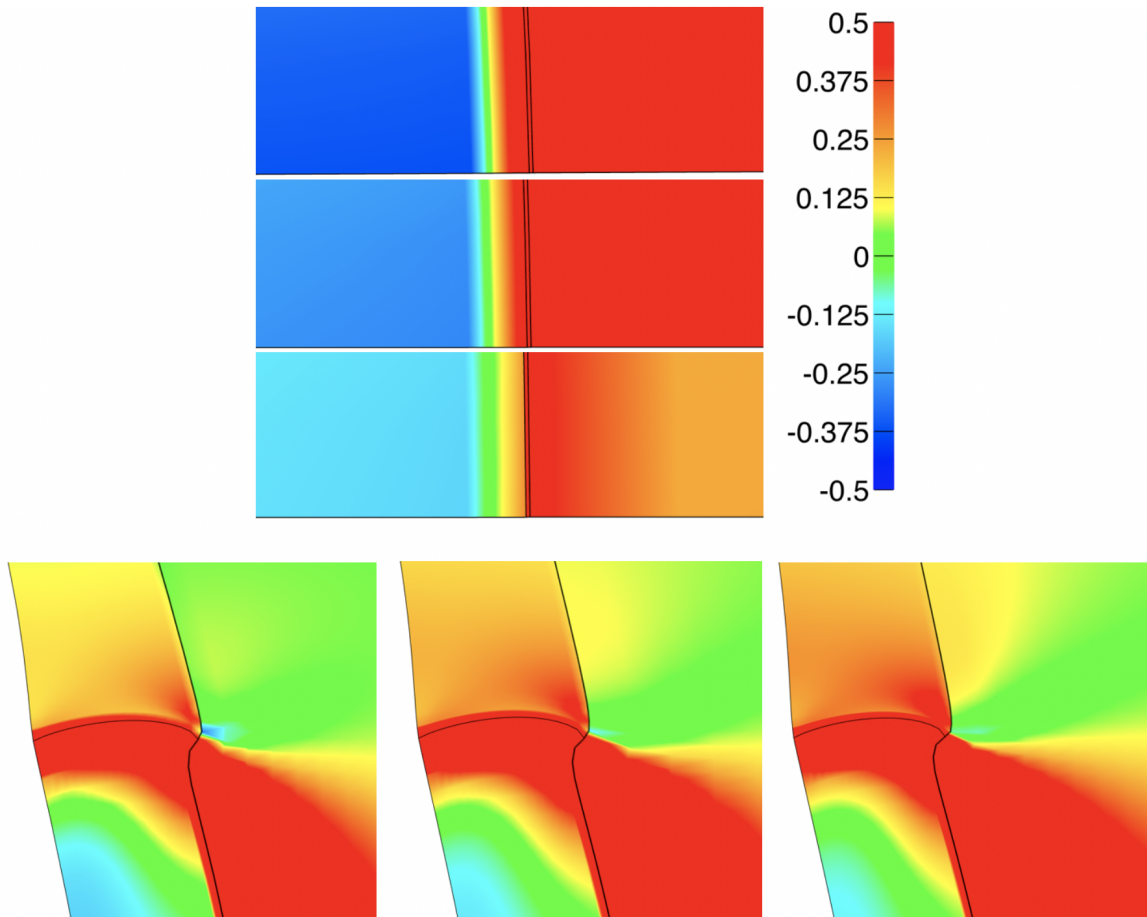


Figure 3.6. Results of study into effect of duct radius. 1st principal stresses at end time point [kPa] - top 3 images show the radial stress profile at the bottom edge of model for (top to bottom) 1 mm lumen radius, control case, and 5 mm lumen radius. Bottom 3 images show the stress profile at the intersection point of all domains for (left to right) 1 mm lumen radius, control case, and 5 mm lumen radius.

3.6 Summary of key findings

The key findings of our research are summarized in the histogram in Figure 3.7. Measurements were taken at the end time point of each model case for the maximum 1st principal and shear stresses. As we discuss later, we suspect that the basement membrane will fail when one or both of these quantities exceeds some threshold value. Based on this theory, maximum 1st principal and shear stress values can serve as surrogate indicators of invasive potential.

First we will examine how these values change with basement membrane thickness. Both 1st principal and shear stress increase when the control basement membrane is introduced (compared to a no basement membrane case). When the thickness is increased, both max stresses decrease slightly.

Similarly, when basement membrane stiffness is increased from the control case, both maximum 1st principal and shear stress values increase. However, a stiffer basement membrane will likely have a higher threshold value for rupture. This is also true for basement membrane thickness; while introduction of the basement membrane increases the stresses experienced, it also likely increases the stress that the system can withstand.

Lastly, when the lumen radius is varied among the selected values, it seems that larger ducts impose higher maximum shear stress and lower maximum 1st principal stresses. As we discuss later, this suggests that larger ducts may not be specifically more or less invasive, but rather may experience different outgrowth patterns.

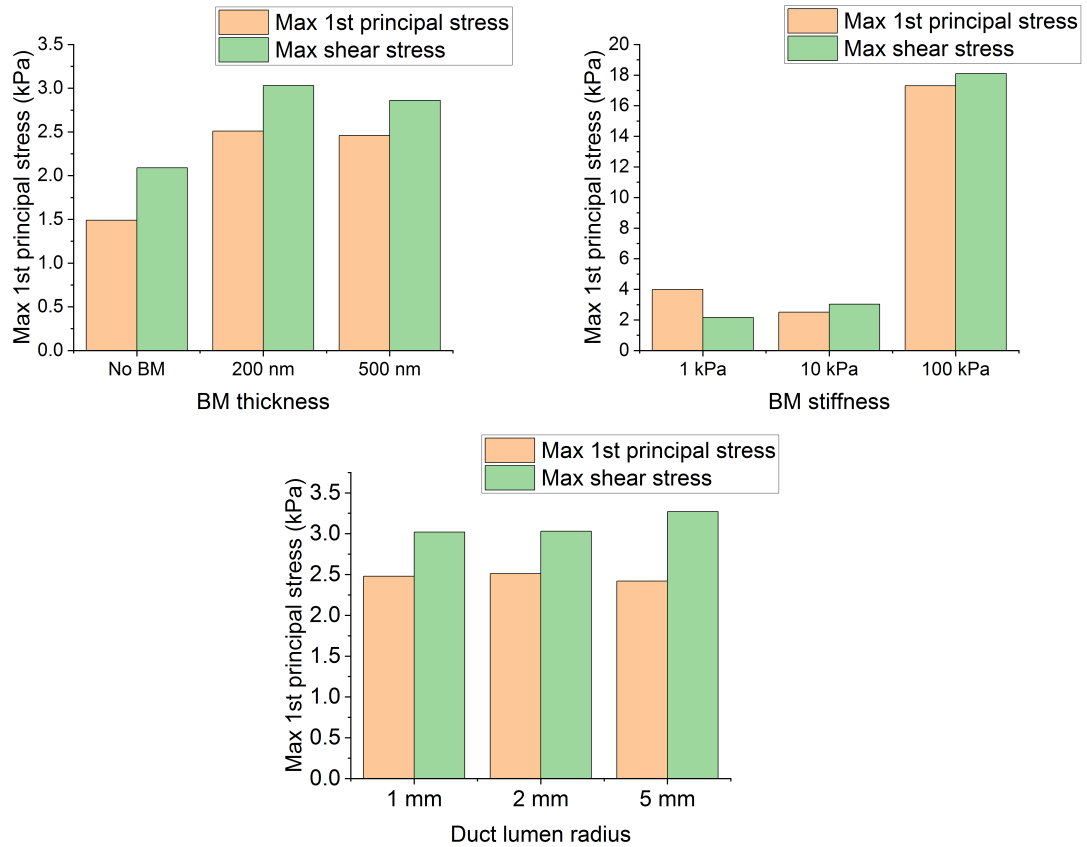


Figure 3.7. Histograms comparing maximum 1st principal and shear stresses observed for each model case.

4. DISCUSSION

There are various reviews in literature which have presented theoretical models of stress distributions in solid tumors. One study postulated that stresses applied on the tumor are purely compressive at the center of the tumor and radially compressive yet circumferentially tensile at the tumor periphery [31]. The results we presented for 1st principal stresses support this suggestion; the tumor region undergoes compression at the center of the region and a layer of tension around the edges.

We have constructed a model of the major mechanical forces associated with the development and growth of epithelial tumors. This model has been used to demonstrate a probable distribution of stresses throughout the surrounding environment and we have explored the relative impacts of various parameters. Another significant contribution is that we model our tumor with a reasonably accurate (although simplified) shape. Most studies, particularly those done *in vitro*, model tumors as spherical agglomerations of cancer cells. However, as discussed in the introduction and shown in Figure 1.1, epithelial tumors *in vivo* are not spherical at all but rather are curved around a hollow epithelial duct.

This model is able to address some of the limitations mentioned previously, especially regarding the combination pro- and anti-tumorigenic role of the basement membrane and stroma. By employing a computational model, we were able to isolate the effects of individual components and properties. Specifically, our results indicate that increased basement membrane stiffness and thickness, although they restrain outward displacement of the tumor, increase normal stresses on the stroma. Additionally, they indicate that tumors in smaller ducts inflict more normal stresses and less shear stresses. It would not be possible to isolate these effects in a traditional *in vitro* or animal study.

While we believe these contributions are significant, the model is not without limitations. First, it is important to note that while this model does yield some quantitative data, these numbers are only rough approximations and should be treated as such. The primary value is in the qualitative findings regarding the distribution of stresses and relative impact of various parameters.

Next, the model is limited by the assumption of bonded interfaces between all regions. Contacts between neighboring material regions are modeled by welding adjacent nodes together. In contrast with this, epithelial cell-basement membrane adhesion is mediated *in vivo* by several factors including a protein called dystroglycan. Research shows that during tissue growth or remodeling phases, these interfaces are detached to allow for free sliding [32]. Similarly, it has been shown that dystroglycan expression is reduced in a variety of human cancers, especially in advanced cases [33]. These observations indicate that a free sliding interface or one that slides with some friction coefficient may be more realistic as a subject of potential future works.

All material properties are assumed constant over time, with the exception of the cancer swelling and the cases which involved basement membrane degradation. This is likely an oversimplification, as the tumor microenvironment is highly dynamic and changes drastically between healthy and disease states. As described above, properties of the material regions used in the model were chosen based on literature values for a diseased state, without consideration for how far the disease has progressed.

The stroma is modeled as a uniform, linearly elastic isotropic material region. In reality, this region is highly heterogeneous and composed of various components as mentioned in the Introduction and shown in Figure 1.1. Thus, it is a somewhat significant simplification to model it as homogeneous and isotropic.

Lastly, as shown in Figure 1.1, the epithelial layer is not perfectly homogeneous either but rather is composed of a single layer of cells with distinct nuclei. Cell nuclei are known to be much stiffer and less compressible than their surrounding cytoplasm. This likely means that *in vivo*, the epithelial layer is not capable of being compressed

linearly and indefinitely but rather would reach some maximum compression point at which the neighboring nuclei are effectively touching.

5. CONCLUSION

The findings presented above shed some light on the mechanisms underlying the development, growth and invasion of epithelial cancer tumors. We have explored how various parameters affect the propagation of stresses into the stroma, which may induce a molecular signaling response. Most significantly, we observe that the majority of normal stress is concentrated within the basement membrane layer. Based on this, we hypothesize that there is some critical axial stress that the basement membrane can undergo, with basement membrane rupture and subsequent invasion occurring when this threshold is exceeded. Similarly, there may be a critical shear stress at the epithelium-basement membrane interface beyond which the epithelium will dislocate from the basement membrane and be able to grow more freely. Based on this, analysis of how various parameters affect both the stress propagation and the maximum axial stress on the basement membrane and maximum shear stress at the epithelium-basement membrane interface may allow for some qualitative prediction of tumor progression and tissue response.

REFERENCES

REFERENCES

- [1] Kleeff, Jorg, Murray Korc, Minoti Apte, Carlo La Vecchia, Colin D. Johnson, Andrew V. Biankin, Rachel E. Neale, et al. “Pancreatic Cancer.” *Nature Reviews Disease Primers* 2, no. 1 (April 21, 2016). <https://doi.org/10.1038/nrdp.2016.22>
- [2] Siegel, Rebecca L., Kimberly D. Miller, and Ahmedin Jemal. “Cancer Statistics, 2015.” *CA: A Cancer Journal for Clinicians* 65, no. 1 (January 2015): 5–29. <https://doi.org/10.3322/caac.21254>
- [3] Mihaljevic, André L., Christoph W. Michalski, Helmut Friess, and Jörg Kleeff. “Molecular Mechanism of Pancreatic Cancer—Understanding Proliferation, Invasion, and Metastasis.” *Langenbecks Archives of Surgery* 395, no. 4 (2010): 295–308. <https://doi.org/10.1007/s00423-010-0622-5>.
- [4] Olive, K. P., M. A. Jacobetz, C. J. Davidson, A. Gopinathan, D. McIntyre, D. Honess, B. Madhu, et al. “Inhibition of Hedgehog Signaling Enhances Delivery of Chemotherapy in a Mouse Model of Pancreatic Cancer.” *Science* 324, no. 5933 (2009): 1457–61. <https://doi.org/10.1126/science.1171362>.
- [5] Feldmann, G, N Habbe, S Dhara, S Bisht, H Alvarez, V Fendrich, R Beaty, et al. “Hedgehog Inhibition Prolongs Survival in a Genetically Engineered Mouse Model of Pancreatic Cancer.” *Gut* 57, no. 10 (2008): 1420–30. <https://doi.org/10.1136/gut.2007.148189>.
- [6] Erkan, Mert, Christoph W. Michalski, Simon Rieder, Carolin Reiser–Erkan, Ivane Abiatari, Armin Kolb, Nathalia A. Giese, Irene Esposito, Helmut Friess, and Jörg Kleeff. “The Activated Stroma Index Is a Novel and Independent Prognostic Marker in Pancreatic Ductal Adenocarcinoma.” *Clinical Gastroenterology and Hepatology* 6, no. 10 (2008): 1155–61. <https://doi.org/10.1016/j.cgh.2008.05.006>.
- [7] Stylianopoulos, T., J. D. Martin, V. P. Chauhan, S. R. Jain, B. Diop-Frimpong, N. Bardeesy, B. L. Smith, et al. “Causes, Consequences, and Remedies for Growth-Induced Solid Stress in Murine and Human Tumors.” *Proceedings of the National Academy of Sciences* 109, no. 38 (2012): 15101–8. <https://doi.org/10.1073/pnas.1213353109>.
- [8] Cheng, Gang, Janet Tse, Rakesh K. Jain, and Lance L. Munn. “Micro-Environmental Mechanical Stress Controls Tumor Spheroid Size and Morphology by Suppressing Proliferation and Inducing Apoptosis in Cancer Cells.” *PLoS ONE* 4, no. 2 (2009). <https://doi.org/10.1371/journal.pone.0004632>.
- [9] Demou, Zoe N. “Gene Expression Profiles in 3D Tumor Analogs Indicate Compressive Strain Differentially Enhances Metastatic Potential.” *Annals of Biomedical Engineering* 38, no. 11 (2010): 3509–20. <https://doi.org/10.1007/s10439-010-0097-0>.

- [10] Tse, J. M., G. Cheng, J. A. Tyrrell, S. A. Wilcox-Adelman, Y. Boucher, R. K. Jain, and L. L. Munn. “Mechanical Compression Drives Cancer Cells toward Invasive Phenotype.” *Proceedings of the National Academy of Sciences* 109, no. 3 (2011): 911–16. <https://doi.org/10.1073/pnas.1118910109>.
- [11] Helmlinger, Gabriel, Fan Yuan, Marc Dellian, and Rakesh K. Jain. “Interstitial PH and pO₂ Gradients in Solid Tumors in Vivo: High-Resolution Measurements Reveal a Lack of Correlation.” *Nature Medicine* 3, no. 2 (1997): 177–82. <https://doi.org/10.1038/nm0297-177>.
- [12] Liu, Tianyi, Linli Zhou, Danni Li, Thomas Andl, and Yuhang Zhang. “Cancer-Associated Fibroblasts Build and Secure the Tumor Microenvironment.” *Frontiers in Cell and Developmental Biology* 7 (April 24, 2019). <https://doi.org/10.3389/fcell.2019.00060>
- [13] Huang, Tu-Xiong, Xin-Yuan Guan, and Li Fu. “Therapeutic Targeting of the Crosstalk Between Cancer-Associated Fibroblasts and Cancer Stem Cells”. *American Journal of Cancer Research* 9, no. 9 (September 1, 2019). <https://www.ncbi.nlm.nih.gov/pmc/articles/PMC6780671/>
- [14] Bussard, Karen M., Lysette Mutkus, Kristina Stumpf, Candelaria Gomez-Manzano, and Frank C. Marini. “Tumor-Associated Stromal Cells as Key Contributors to the Tumor Microenvironment.” *Breast Cancer Research* 18, no. 1 (August 11, 2016). <https://doi.org/10.1186/s13058-016-0740-2>
- [15] Ishii, Genichiro, Atsushi Ochiai, and Shinya Neri. “Phenotypic and Functional Heterogeneity of Cancer-Associated Fibroblast within the Tumor Microenvironment.” *Advanced Drug Delivery Reviews* 99 (2016): 186–96. <https://doi.org/10.1016/j.addr.2015.07.007>.
- [16] Kraman, M., P. J. Bamburg, J. N. Arnold, E. W. Roberts, L. Magiera, J. O. Jones, A. Gopinathan, D. A. Tuveson, and D. T. Fearon. “Suppression of Antitumor Immunity by Stromal Cells Expressing Fibroblast Activation Protein-.” *Science* 330, no. 6005 (April 2010): 827–30. <https://doi.org/10.1126/science.1195300>.
- [17] Gaggioli, Cedric, Steven Hooper, Cristina Hidalgo-Carcedo, Robert Grosse, John F. Marshall, Kevin Harrington, and Erik Sahai. “Fibroblast-Led Collective Invasion of Carcinoma Cells with Differing Roles for RhoGTPases in Leading and Following Cells.” *Nature Cell Biology* 9, no. 12 (2007): 1392–1400. <https://doi.org/10.1038/ncb1658>.
- [18] Flaberg, Emilie, Laszlo Markasz, Gabor Petranyi, Gyorgy Stuber, Ferenc Dicsó, Nidal Alchihabi, Èva Oláh, et al. “High-Throughput Live-Cell Imaging Reveals Differential Inhibition of Tumor Cell Proliferation by Human Fibroblasts.” *International Journal of Cancer* 128, no. 12 (2010): 2793–2802. <https://doi.org/10.1002/ijc.25612>.
- [19] Maas, Steve A., Benjamin J. Ellis, Gerard A. Ateshian, and Jeffrey A. Weiss. “FEBio: Finite Elements for Biomechanics.” *Journal of Biomechanical Engineering* 134, no. 1 (January 2012). <https://doi.org/10.1115/1.4005694>.
- [20] Hacl, Stanislaw, Adam Nalecz, Marek Dobosz, Krzysztof Radziszewski, Jacek Reszetow1, Kazimierz Jaskiewicz, and Zbigniew Sledzinski. “Pancreatic Cross-Section: an Elliptical Model”. *Journal of the Pancreas* 8, no.

- 2 (January 3, 2007). <https://pancreas.imedpub.com/pancreatic-crosssection-an-elliptical-model.php?aid=2681>
- [21] Shiner, M., and M. S. C. Birbeck. “The Microvilli of the Small Intestinal Surface Epithelium in Coeliac Disease and in Idiopathic Steatorrhoea.” *Gut* 2, no. 3 (September 1, 1961): 277–84. <https://doi.org/10.1136/gut.2.3.277>
- [22] Tanner, Kandice. “Regulation of the Basement Membrane by Epithelia Generated Forces.” *Physical Biology* 9, no. 6 (November 29, 2012): 65003. <https://doi.org/10.1088/1478-3975/9/6/065003>
- [23] Ateshian, Gerard A., Kevin D. Costa, Evren U. Azeloglu, Barclay Morrison III, and Clark T. Hung. “Continuum Modeling of Biological Tissue Growth by Cell Division, and Alteration of Intracellular Osmolytes and Extracellular Fixed Charge Density.” *Journal of Biomechanical Engineering* 131, no. 10 (September 1, 2009). <https://doi.org/10.1115/1.3192138>
- [24] Nakamura, Tsukasa, Koji Masuda, Shumpei Harada, Kiyokazu Akioka, and Hirotaka Sako. “Pancreatic Cancer: Slow Progression in the Early Stages.” *International Journal of Surgery Case Reports* 4, no. 8 (2013): 693–96. <https://doi.org/10.1016/j.ijscr.2013.04.040>
- [25] Guo, Xinyi, Keith Bonin, Karin Scarpinato, and Martin Guthold. “The Effect of Neighboring Cells on the Stiffness of Cancerous and Non-Cancerous Human Mammary Epithelial Cells.” *New Journal of Physics* 16, no. 10 (October 6, 2014): 105002. <https://doi.org/10.1088/1367-2630/16/10/105002>
- [26] Rice, A J, E Cortes, D Lachowski, B C H Cheung, S A Karim, J P Morton, and A del Río Hernández. “Matrix Stiffness Induces Epithelial–mesenchymal Transition and Promotes Chemoresistance in Pancreatic Cancer Cells.” *Oncogenesis* 6, no. 7 (July 2017): e352–e352. <https://doi.org/10.1038/oncsis.2017.54>
- [27] Chlasta, Julien, Pascale Milani, Gaël Runel, Jean-Luc Duteyrat, Leticia Arias, Laurie-Anne Lamiré, Arezki Boudaoud, and Muriel Grammont. “Variations in Basement Membrane Mechanics Are Linked to Epithelial Morphogenesis.” *Development* 144, no. 23 (October 16, 2017): 4350–62. <https://doi.org/10.1242/dev.152652>
- [28] Dabhere, V C, and D V Bhope. “Investigation of Stresses in Bi-material Strip Subjected to Constant Temperature and Temperature Gradient by FEM.” *Int. J. Engg. Res. Sci. Tech.* 4, no. 3 (August 2015).
- [29] Messal, Hendrik A., Silvanus Alt, Rute M. M. Ferreira, Christopher Gribben, Victoria Min-Yi Wang, Corina G. Cotoi, Guillaume Salbreux, and Axel Behrens. “Tissue Curvature and Apicobasal Mechanical Tension Imbalance Instruct Cancer Morphogenesis.” *Nature* 566, no. 7742 (January 30, 2019): 126–30. <https://doi.org/10.1038/s41586-019-0891-2>
- [30] Banan, M.r., G. Karami, and M. Farshad. “Finite Element Stability Analysis of Curved Beams on Elastic Foundation.” *Mathematical and Computer Modelling* 14 (1990): 863–67. [https://doi.org/10.1016/0895-7177\(90\)90304-6](https://doi.org/10.1016/0895-7177(90)90304-6).
- [31] Jain, Rakesh K., John D. Martin, and Triantafyllos Stylianopoulos. “The Role of Mechanical Forces in Tumor Growth and Therapy.” *Annual Review of Biomedical Engineering* 16, no. 1 (November 2014): 321–46. <https://doi.org/10.1146/annurev-bioeng-071813-105259>.

- [32] McClatchey, Shelly T.H., Zheng Wang, Lara M Linden, Eric L. Hastie, Lin Wang, Wanqing Shen, Alan Chen, Qiuyi Chi, and David R Sherwood. "Boundary Cells Restrict Dystroglycan Trafficking to Control Basement Membrane Sliding During Tissue Remodeling". *eLife* 5 (September 23, 2016). <https://doi.org/10.7554/eLife.17218>
- [33] Sgambato, A., A. Camerini, D. Amoroso, G. Genovese, F. De Luca, M. Cecchi, M. Migaldi, et al. "Expression of Dystroglycan Correlates with Tumor Grade and Predicts Survival in Renal Cell Carcinoma." *Cancer Biology and Therapy* 6, no. 12 (December 2007): 1840–46. <https://doi.org/10.4161/cbt.6.12.4983>